Peptides 84 (2016) 44–57

Contents lists available at ScienceDirect

Peptides

journal homepage: www.elsevier.com/locate/peptides

Hydrocarbon stapled B chain analogues of relaxin-3 retain biological activity

Tharindunee Jayakody[a,b,c,1], Subhi Marwari[a,d,1], Rajamani Lakshminarayanan[e,f], Francis Chee Kuan Tan[a], Charles William Johannes[g], Brian William Dymock[d], Anders Poulsen[h], Deron Raymond Herr[a], Gavin Stewart Dawe[a,b,c,*]

[a] Department of Pharmacology, Yong Loo Lin School of Medicine, National University of Singapore, Singapore
[b] Neurobiology and Ageing Programme, Life Sciences Institute, National University of Singapore, Singapore
[c] Singapore Institute for Neurotechnology (SINAPSE), National University of Singapore, Singapore
[d] Department of Pharmacy, Faculty of Science, National University of Singapore, Singapore
[e] Singapore Eye Research Institute, Singapore
[f] Ophthalmology and Visual Sciences Academic Clinical Program, Duke-NUS Medical School, Singapore
[g] Institute of Chemical and Engineering Sciences, Agency for Science, Technology and Research (A*STAR), Singapore
[h] Department of Medicinal Chemistry, Experimental Therapeutics Centre, Agency for Science, Technology and Research (A*STAR), Singapore

ARTICLE INFO

Article history:
Received 24 December 2015
Received in revised form 29 July 2016
Accepted 2 August 2016
Available online 3 August 2016

Keywords:
Relaxin-3
INSL7
RXFP3
Stapled peptide
ERK1/2
cAMP

ABSTRACT

Relaxin-3 or insulin-like peptide 7 (INSL7) is the most recently discovered relaxin/insulin-like family peptide. Mature relaxin-3 consists of an A chain and a B chain held by disulphide bonds. According to structure activity relationship studies, the relaxin-3 B chain is more important in binding and activating the receptor. RXFP3 (also known as Relaxin-3 receptor 1, GPCR 135, somatostatin- and angiotensin- like peptide receptor or SALPR) was identified as the cognate receptor for relaxin-3 by expression profiles and binding studies. Recent studies imply roles of this system in mediating stress and anxiety, feeding, metabolism and cognition. Stapling of peptides is a technique used to develop peptide drugs for otherwise undruggable targets. The main advantages of stapling include, increased activity due to reduced proteolysis, increased affinity to receptors and increased cell permeability. Stable agonists and antagonists of RXFP3 are crucial for understanding the physiological significance of this system. So far, agonists and antagonists of RXFP3 are peptides. In this study, for the first time, we have introduced stapling of the relaxin-3 B chain at 14th and 18th positions (14s18) and 18th and 22nd position (18s22). These stapled peptides showed greater helicity than the unstapled relaxin-3 B chain in circular dichroism analysis. Both stapled peptides bound RXFP3 and activated RXFP3 as observed in an inhibition of forskolin-induced cAMP assay and a ERK1/2 activation assay, although with different potencies. Therefore, we conclude that stapling of the relaxin3 B chain does not compromise its ability to activate RXFP3 and is a promising method for developing stable peptide agonists and antagonists of RXFP3 to aid relaxin-3/RXFP3 research.

© 2016 The Author(s). Published by Elsevier Inc. This is an open access article under the CC BY-NC-ND license (http://creativecommons.org/licenses/by-nc-nd/4.0/).

1. Introduction

Relaxin-3 or insulin-like peptide 7 (INSL7) is the most recently discovered insulin/insulin-like growth factor/relaxin family neuropeptide [1]. Phylogenetic analyses have suggested relaxin-3 to be the likely ancestor of the relaxin family as it is conserved from fish to mammals [2]. Relaxin-3 consists of an A chain (24 amino acids) and a B chain (27 amino acids) held together by two inter-chain disulphide bonds and one intra-A chain disulphide bond [3]. According to structure activity relationship studies, relaxin-3 interacts with its cognate receptor, the RXFP3 receptor, mainly through the R*XXX*R*XX*(I/V) motif of the B chain [1,4]. Relaxin-3 also binds and activates RXFP4 and RXFP1 [5]. In the mouse, rat and macaque, high levels of relaxin-3 expression have been observed in the brainstem nucleus in the ventromedial dorsal tegmental area commonly known as the nucleus

* Corresponding author at: Department of Pharmacology, Yong Loo Lin School of Medicine, National University of Singapore, Building MD3, #04-01, 16 Medical Drive, Singapore 117600, Singapore.
E-mail address: gavin_dawe@nuhs.edu.sg (G.S. Dawe).
[1] These two authors contributed equally.

http://dx.doi.org/10.1016/j.peptides.2016.08.001
0196-9781/© 2016 The Author(s). Published by Elsevier Inc. This is an open access article under the CC BY-NC-ND license (http://creativecommons.org/licenses/by-nc-nd/4.0/).

incertus, compared to peripheral tissues [1,6–8]. Projections from the nucleus incertus have been extensively studied in the rat [9–12].

RXFP3 (previously also known as RXFP Receptor 3, Relaxin-3 receptor 1, GPCR135, somatostatin- and angiotensin- like peptide receptor or SALPR), a product of a single copy intronless gene, was identified as the cognate receptor for relaxin-3 by expression profiles and binding studies [6,9,10]. In the mouse and the macaque, RXFP3 expression has been observed mainly in the brain, and more discrete RXFP3 expression has been detected in rat hypothalamic areas such as the paraventricular nucleus and the supraoptic nucleus [1,6–8,13]. RXFP3 is a class A, rhodopsin-like GPCR with a short N-terminal extracellular domain [14]. When stimulated with human relaxin-3 (H3 relaxin), RXFP3 couples to $G_{\alpha i}$ proteins inhibiting cAMP accumulation in RXFP3 stably expressing CHO-K1 cells (CHO-RXFP3) [6,15,16]. In RXFP3 stably expressing HEK293 cells (HEK-RXFP3) transiently transfected with G_{qi5}, Ca^{2+} mobilization was observed when stimulated by H3 relaxin [6,17]. In a separate study using HEK-RXFP3 and CHO-RXFP3 cells, RXFP3 activation by H3 relaxin activated ERK1/2 via the activation of $G_{\alpha i}$, PI3K, PKC, receptor internalization or compartmentalization into lipid rich environments, and activation of Src tyrosine kinase. Even though these signalling events were common in both cell lines, events such as EGFR transactivation and activation of PLCβ were observed in HEK-RXFP3 cells and not in CHO-RXFP3 cells. Moreover, the latter signalling events were also observed in the murine SN56 cell line [15].

The conserved distribution of the relaxin-3 and RXFP3 system together with behavioural and biochemical studies implies roles for this system in mediating stress and anxiety [18,19], feeding and metabolism [20–25] and cognition [26,27]. Thus, stable agonists and antagonists of RXFP3 will be excellent tools for understanding the mechanism behind these responses and treating stress, feeding and cognition related disorders associated with the relaxin-3/RXFP3 system. Recent advances in developing agonists and antagonists of RXFP3 include a small molecule allosteric modulator of RXFP3 that functions only with the non-native amidated form of the orthosteric agonist H3 relaxin [28] and so has limited utility as a drug, and the development and uses of chimeric peptide agonists and antagonists, and peptide agonists with C-terminally truncated B chains [29–32]. Being peptides, most of these ligands have low stability due to degradation by proteases. Moreover, peptide ligands can only be administered via intracerebroventricular injections to target the CNS, as systemically administered peptides may not cross the blood brain barrier. In this context, hydrocarbon stapling of peptide ligands will be a useful method of developing peptide drugs to overcome challenges faced in targeting the CNS, as stapled peptides, locked in their conformations are highly stable and less prone to proteolytic degradation and are able to efficiently penetrate cells [33]. As mentioned previously, relaxin-3 activates RXFP3 by its B chain, and the A chain acts as a scaffold to stabilize or "staple" the α-helix of the B chain (Fig. 1A and Ci) [4]. Thus we hypothesized that the B chain of relaxin-3 may be stabilized in its α-helical conformation with the use of hydrocarbon stapling which will mimic the presence of the A chain.

Here we report, stapling of the relaxin-3 B chain and testing the stapled peptides for their biological activity. We employed optical dichroism, ligand binding assays, signalling assays based on RXFP3 coupling to $G_{\alpha i/o}$ and ERK1/2 activation to assess the secondary structure and thermal stability of stapled B chains of relaxin-3 and their ability to bind and activate RXFP3. Some of the results reported here were previously communicated in a meeting abstract [34].

2. Materials and methods

2.1. Materials

RXFP3 stably expressing HEK293T cells (HEK-RXFP3), CHO-K1 cells (CHO-RXFP3) and RXFP3 endogenously expressing SN56 cells were provided by Prof. Roger Summers (Monash Institute of Pharmaceutical Sciences & Department of Pharmacology, Monash University) and Prof. Ross Bathgate (Florey Institute of Neuroscience and Mental Health, University of Melbourne). HEK293T (wild type) cells were provided by Prof. Lawrence Stanton (Genome Institute of Singapore). Human relaxin-3 (H3 relaxin) was purchased from Peprotech Inc. (cat. no.130-10, USA). DMEM, TripLE, Hygromycin B was from Life Technologies (USA), fetal bovine serum (FBS) was from Life Technologies (South America), poly-L-lysine (PLL), 3-isobutyl-1-methylxanthine (IBMX) and bovine serum albumin (BSA) were from Sigma (Saint Louis, USA). Dimethyl sulfoxide (DMSO) was from MP Biomedicals (Solon-Ohio, USA). Forskolin was from Tocris Bioscience (Bristol, UK), The cyclic AMP (cAMP) enzyme immunoassay (EIA) kit was from Cayman Chemicals (Ann Arbor, MI), and hydrochloric acid (HCl) was from BDH Chemicals Ltd. (UK). Sodium dodecyl sulphate (SDS) lysis buffer (4x) was prepared using 2 M dithiothreitol to a final concentration of 0.4 M (Goldbiotechnology, USA), 1 M TrisHCl, pH 6.8 to a final concentration of 0.313 (1st BASE, Singapore), 10% SDS (w/v) (Bio-Rad- USA), 50% glycerol (v/v) (Sigma, Saint Louis, USA) and 0.05% (w/v) bromophenol blue (Bio-Rad). Immun-Blot® PVDF membranes were from Bio- Rad (USA), 30% acrylamide and bis-acrylamide solution, 37.5:1 was from Bio-Rad (China), ammonium persulphate were from Bio-Rad (Japan), 1.5 M TrisHCl, pH 8.8, 0.5 M TrisHCl, pH 6.8, tris glycine buffer, tris glycine-SDS buffer, tris-Buffered Saline (TBS) were from 1stBase (Singapore), Tetramethylethylenediamine (TEMED) was from Life Technologies (USA). Tween 20 was from Sinopharm Chemical Reagent Co, Ltd. (China). Anti-phospho p44/p42 MAPK (ERK1/2) (Cat. No. 4370S) and anti-p44/p42 MAPK (ERK1/2) (Cat. No. 4370S) were from Cell Signalling Technology. Goat anti-rabbit HRP conjugated secondary antibodies (cat. no. 31460) were purchased from Thermo Scientific. Luminata forte western HRP substrate was from Merk Millipore (Billeria, MA, USA). Restore™ Western blot striping buffer was from Thermo Fischer Scientific (Rockford, USA). Cell culture flasks and plates were from Greiner Bio-One (Germany).

2.2. Designing and modelling of the stapled peptides

Relaxin-3 binds to RXFP3 by R*XXX*R*XX*(I/V) motif of the B chain [1]. Moreover residues R8, R12, I15, R16, and F20 of the relaxin-3 B chain helix are reported to be important in binding to RXFP3 and C terminal residues R26 and W27 are important in activating the receptor (Fig. 1Cii) [32,35]. Based on this knowledge, we designed two stapled peptides which were stapled at 18th and 22nd positions (18s22) (Fig. 1Civ) and 14th and 18th positions (14s18) (Fig. 1Cv). Residues involved in stapling were chosen so that they will not interfere with residues important in receptor binding and activation and to mimic the disulphide bond formation of the A chain in the native relaxin-3. Cys residues at positions 10 and 22 were mutated to Ser to prevent cyclization and oligomerization of the peptides. A corresponding relaxin-3 B chain double mutant (Fig. 1Cii) was synthesised as an unstapled peptide control.

The nuclear magnetic resonance (NMR) structure of relaxin-3 (PDB entry 2FHW) [36] was prepared using the Protein Preparation Wizard in Maestro version 10.3 (Schrodinger LLC, New York, USA]). This preparation process is necessary to ensure structural correctness. NMR analysis produces a set of estimates of constraints on distances between atoms resulting in an ensemble of models rather than a single structure. The 2FHW structural ensemble

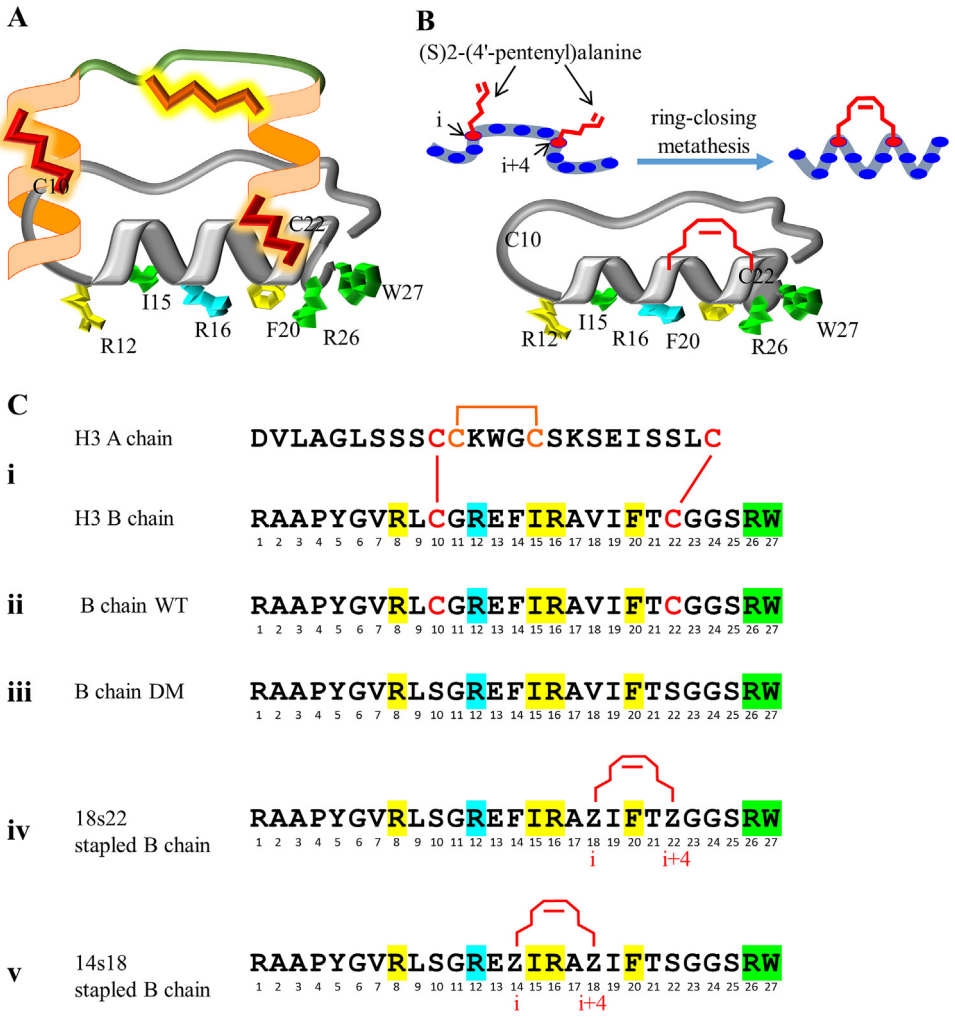

Fig 1. (A) Schematic representation of ribbon structure of relaxin-3. (B) Strategy for designing the stapled B chains of relaxin-3 by ring-closing metathesis to staple the α-helix of the B chain of relaxin-3 by i and i + 4 stapling. (C) (i) Sequence of the A and B chains of human relaxin-3 (H3) held by two inter-chain disulphide bonds and one intra-A chain disulphide bond; (ii) sequence of the wild type B chain of relaxin-3 (B chain WT); (iii) sequence of the relaxin-3 B chain Cys10Ser + Cys22Ser double mutant (B chain DM); (iv) sequence of the 18s22 stapled B chain of relaxin-3 stapled at 18th and 22nd position by i and i + 4 stapling (18s22); and (v) sequence of the 14s18 stapled B chain of relaxin-3 stapled at 14th and 18th position by i and i + 4 stapling (14s18). Residues highlighted in green are involved in RXFP3/RXFP4 activation, residues highlighted in yellow are involved in RXFP3/RXFP4 binding, while residues highlighted in blue are involved in RXFP3 binding only [35]. (For interpretation of the references to color in this figure legend, the reader is referred to the web version of this article.)

contains 20 such models for relaxin-3. The preparation process included setting the tautomer and protonation state of the peptide and subjecting each of the 20 structures to restrained minimization using an optimized potentials for liquid simulations (OPLS) force field [37], specifically the OPLS3 force field optimized to provide broad coverage of drug-like small molecules and proteins [38], and a generalized Born model of solvation augmented with the hydrophobic solvent accessible surface area term (GB/SA solvation model). Structures 1, 10 and 20 were selected for molecular dynamics (MD) simulations using both intact relaxin-3 with the A and B chains together or the B chain only. Both the wild type relaxin-3 B chain and a relaxin-3 B chain Cys10Ser + Cys22Ser double mutant (double mutant) (Fig. 1Ciii) were investigated. The Desmond System Builder version 4.3 (Schrodinger LLC) was used to build a solvated system for the simulation including the solute peptide and the solvent water molecules with counter ions. We used that flexible simple point charge (SPC) water model for the solvent with orthorhombic boundary conditions and a 10 Å buffer. The systems were neutralized with Cl^- ions and 0.15 M NaCl salt was added. The systems were then relaxed and subjected to 12 ns MD using the OPLS3 force field and a substance (N), pressure (P) and temperature (T) [NPT] ensemble class with T = 300 K and P = 1.01325 bar. The stapled peptides were built using the relaxin-3 B chain Cys10Ser + Cys22Ser double mutant of structures 1, 10 and 20 of the 2FHW structural ensemble and prepared as described above. The staple and the two amino acids involved in stapling were relaxed using 200 steps of Polak-Ribiere conjugate gradient (PRCG) minimization, the OPLS3 force field and the GB/SA solvation model while the remaining residues were constrained. Systems were then build and these were subjected to 12 ns MD as described above.

2.3. Stapled peptides

Hydrocarbon stapling of the designed relaxin-3 B chains was carried out by substituting the amino acids at *i*(14) and *i* + 4(18) positions or *i*(18) and *i* + 4(22) positions with (S)2-(4′-pentenyl)alanine and subsequent ring-closing metathesis (RCM). Biosynthesis Inc. (USA) was contracted to synthesise these peptides. The molecular weight and purity of the peptides were analysed by mass spectrometry and RP- HPLC by Biosynthesis Inc. (USA).

2.4. Circular dichroism

Circular dichroism (CD) experiments were carried out using a Jasco 815 spectrometer (Tokyo, Japan). The final peptide concentration was kept constant (0.20 mg/ml) for all the peptides studied. To determine the α-helicity of the synthesised peptide samples, CD spectra were collected from 190 to 260 nm using a 0.1 cm path length quartz cuvette at room temperature. We used a continuous scan with a 20 nm/min scanning speed with a response time of 0.5 s, 0.5 nm step resolution and 1 nm spectral band width. All peptide samples were measured in water with the peptide concentration ranging from 50 to 65 μM. The spectra were generated as an average of 3 independent scans. After baseline correction, the final spectra were expressed as a molar ellipticity θ (deg cm^2 $dmol^{-1}$) per residue. All spectra were converted to a uniform scale of molar ellipticity after background subtraction. Curves shown are smoothed with standard parameters.

The mean helical content of the peptide samples was calculated using the mean residual ellipticity at 222 nm:

$$\%\text{helicity} = 100[\theta_{222\,\text{nm}}/(40,000(1-2.5/n))]$$

where n is the number of amino acid and $\Theta_{222\text{nm}}$ is the mean residual ellipticity at 222 nm [39–41].

2.5. Variable temperature circular dichroism

The variable temperature CD (VT-CD) experiments were performed on a Jasco J-815 spectropolarimeter equipped with a peltier set up. The peptides were dissolved in water with the concentration ranging from 50 to 65 μM. A quartz cuvette with the path length of 0.1 cm was used. For the wavelength scan, spectra were monitored over the 190–260 nm range with a resolution of 0.2 nm and a band width of 1 nm. Temperature-dependent CD spectra of each peptide were scanned at 5 °C intervals over a temperature range of 20–90 °C from 190 to 260 nm. To generate thermal unfolding curves, the ellipticity at 222 nm was measured every 5 °C from 20 to 90 °C with a temperature slope of 1 °C/min. Experiments at each temperature were recorded after 30 min to allow for equilibrium in the sample cell. The spectra presented are an average of 3 independent scans with a scan speed of 20 nm/min. Replicate measurements as a function of temperature reproduced the spectra within ±5% after the heating cycle. For the single wavelength measurements at 222 nm, the heating rate was 0.5 °C/min over a temperature range of 20–90 °C and 90–20 °C [42].

2.6. Characterization of unfolding by following the change in ellipticity at a single wavelength As a function of temperature

When the CD of a protein changes as a function of temperature, the change is utilized to analyse the thermodynamics of unfolding or folding. In the simplest case, a molecule undergoes an unfolding transition between two states: folded, F, and unfolded, U. At any temperature, T, the constant of folding is, K, is:

$$K = [F]/[U]$$

[F] and [U] are the concentrations of the folded and unfolded forms respectively. The fraction folded at any temperature is α.

$$\alpha = [F]/([F] + [U])$$

$$\alpha = (\Theta_t - \Theta_U)/(\Theta_F - \Theta_U)$$

Θ_t is the observed ellipticity at any temperature, Θ_F is the ellipticity of the fully folded form and Θ_U is the ellipticity of the unfolded form. To fit the change of CD at a single wavelength as a function of temperature, T (Kelvin), the Gibbs–Helmholtz equation that describes the folding as a function of temperature was applied [43–46].

2.7. Assay for proteolytic stability of peptides

14s18 (3014.49 Da) and B chain DM (3010.18 Da) peptides reconstituted in water with 0.1% of BSA (66.5 kDa) were digested with sequencing grade endoproteinase Glu-C (glutamly endopeptidase, EC 3.4.21.9; Promega, Madison WI, USA) in a 1:10 enzyme to peptide ratio by incubating for 1 h at 37 °C along with peptide and enzyme only control reactions. The reactions were terminated by adding equal volumes of X2 Tricine Sample Buffer (Bio-Rad, CA, USA) supplemented with 2% v/v β-mercaptoethanol (Sigma) and boiling at 100 °C for five minutes. Products of the digestion and control reactions were then resolved in a 20% Tris-tricine gel and stained by Coomassie Brilliant Blue R-250 staining solution (Bio-Rad, CA, USA) after incubating in a fixing solution composed of 10% acetic acid and 40% Methanol. Coomassie stained gel image was acquired after destaining with Coomassie Brilliant Blue R-250 Destaining Solution (Bio-Rad, USA) [47].

2.8. Cell culture

HEK293T cells stably expressing RXFP3 (HEK-RXFP3), CHO-K1 cells stably expressing RXFP3 (CHO-RXFP3), HEK293T (wild type), CHO-K1 (wild type) and SN56 cells were maintained in DMEM, 10% (v/v) FBS and 1× penicillin/streptomycin (10,000 U/ml) at 37 °C in a 5% CO_2 humidified environment. Each cell line was passaged using TripLE at 80% confluency. In addition, hygromycin B (400 ng/ml) was used to supplement media used in maintaining CHO-RXFP3 cells. For performing the receptor-ligand binding assays and protein estimation, HEK-RXFP3 cells were harvested at 90% cell confluency for plating onto PLL pre-coated 96-well plates.

2.9. Receptor binding assay

2.9.1. Peptide synthesis and characterization

R3 B1-22R peptide was prepared by Fmoc-based solid phase peptide synthesis using standard methods with single coupling reactions and purified using RP-HPLC resulting in a high purity (>95%) product (Biosynthesis Inc., USA). The lanthanide chelating agent, DTPA (diethylenetriaminepentaacetic acid), was coupled with R3 B1-22R and after purification DTPA-R3 B1-22R was incubated with an excess of $EuCl_3$, until the complex between DTPA and Eu^{+3} was formed. The final peptide product was evaluated by matrix-assisted laser desorption-ionization/time-of-flight reflex mass spectrometry (MALDI-TOF-MS), revealing a 1:1 molar ratio of Eu-DTPA labelling to the R3 B1-22R peptide (observed (m/z) 2998.42, theoretical (m/z) 3145.38). However, during the MALDI-TOF-MS analysis, the Eu(III) group was dissociated partially and therefore 2 peaks were seen. This only occurred during the MALDI-TOF-MS analysis. In contrast, the peptide purified by RP-HPLC displayed a single peak with a high purity profile (>95%) product. The final peptide product Eu-DTPA-R3 B1-22R was solubilised in a triethylaminoacetate buffer (pH ~7), to prevent the liberation of europium from DTPA. The specific activity of Eu-DTPA-R3 B1-22R was estimated to be 1×10^5 fluorescence units (FU)/pmol based on the biological activity of the fraction.

2.9.2. Eu(III)-based ligand binding assays

Cells were plated in 96-well plates at a density of 25,000 cells/well. On the day of experiment, media was aspirated from all wells prior to the addition of the ligands to be tested. Ligands were diluted in binding media (DELFIA L*R binding buffer concentrate 10×, diluted 1:10 containing the following final concentrations: 50 mmol/l Tris-HCl, 5 mmol $MgCl_2$, 25 μmol/l EDTA,

0.2% BSA) and samples were tested in triplicates, unless otherwise noted. Saturation binding assays were carried out as follows: increasing concentrations of Eu-DTPA-R3 B1-22R (0.5–128 nM) peptide were added to the cells and incubated for 2.5 h with gentle shaking (~50 rpm) at room temperature. Non-specific binding was determined in the presence of 1 μM unlabelled R3 B1-22R. After binding at room temperature for 2.5 h, the binding solution was removed and cells were washed twice rapidly (~0.5 s) with ice cold PBS. Following the washing step, the enhancement solution (1244-104, Perkin Elmer) was added directly to the wells (150 μl/well) and the plates were incubated for 30 min at 37 °C prior to reading. The plates were read on a Wallac VICTOR^3 instrument using the standard Eu(III) TRL measurement (340 nm excitation, 400 μsec delay, and emission collection for 400 μs at 615 nm).

For competition binding, eight different concentrations of non-labelled R3 B1-22R (1 pM to 10 μM) and intact human relaxin-3 (H3; 1 pM to 10 μM), and nine different concentrations of relaxin-3 B chain Cys10Ser + Cys22Ser double mutant (B chain DM; 1 pM to 100 μM), 18s22 stapled relaxin-3 B chain (18s22; 1 pM to 100 μM) and the 14s18 stapled relaxin-3 B chain (14s18; 1 pM to 100 μM) and a fixed concentration of Eu-DTPA-R3 B1-22R (8 nM) were utilized using an otherwise identical procedure and conditions to those described above. Each condition was run in triplicate and each experiment was repeated at least three times.

2.10. ERK1/2 activation assay

ERK1/2 activation was detected by a Western blot based method [48]. To determine the time course of ERK1/2 activation by H3 relaxin, HEK-RXFP3, CHO-RXFP3, HEK293T and CHO-K1 cells (5×10^5 cells/well) were plated in 12 well plates with DMEM, 10% FBS and penicillin/streptomycin. The next day, cells were serum starved for 3–4 h in 450 μl of DMEM. After starvation, the cells were treated with 10 nM H3 relaxin for time points ranging from 2 to 35 min to determine the time course of ERK1/2 activation or with the stapled peptides at indicated concentrations. At the end of each time point, the reaction was stopped by immediately lysing the cells using 2× SDS loading buffer. The cells were scraped and lysates were transferred to microfuge tubes in ice. The lysates were boiled at 100 °C for 10 min and electrophoresed through 8% SDS-Polyacrylamide gels for 2 h at 100 V. Next, proteins were transferred to a PVDF membrane for 75 min at 110 V followed by blocking with 5% BSA in TBS/Tween 20 and immunoblotting for total ERK1/2 (tERK1/2) using Anti-p44/p42 MAPK (ERK1/2) diluted 1:1000 in 1% BSA in TBS/Tween 20 and goat anti-rabbit HRP conjugated IgG secondary antibody diluted 1:5000. Protein bands were visualized by chemiluminescence using Luminata Forte HRP substrate. After visualization, primary and secondary antibodies were stripped using Restore™ Western blot striping buffer and reprobed using Anti-phospho p44/p42 MAPK (ERK1/2) diluted 1:1000 and visualized as described above.

2.11. Inhibition of forskolin-induced cAMP assay

The cAMP assay was performed essentially as previously described [49]. Briefly, cells (1×10^5/well) were plated in PLL coated 24 well plates. The following day, cells were serum starved with 225 μl of serum free DMEM for six hours. At the end of starvation, cells were treated in triplicate with H3 relaxin, stapled peptides, or vehicle [15] at indicated concentrations for 5–10 min, and then with forskolin (3–5 μM) or vehicle (control) for 15 min in 37 °C. At the end of the incubation, the cells were lysed by shaking with 50 μl 0.1 M HCl for 20 min after which the cells were scraped and centrifuged at 1000*g* for 10 min to pellet the debris. From the supernatant, 50 μl was applied on the mouse anti-rabbit IgG pre-coated plate and assayed according to the manufacturer's instructions (Cyclic AMP EIA Kit, Cayman Chemicals). To estimate the EC_{50}, intact human relaxin-3 (H3) was applied at six concentrations ranging from 1 pM to 100 nM and relaxin-3 B chain Cys10Ser + Cys22Ser double mutant (B chain DM) and the 14s18 stapled relaxin-3 B chain (14s18) were applied at six concentrations ranging from 100 pM to 10 μM on both HEK-RXFP3 cells and wild type HEK293T cells.

2.12. Data analysis

For the ligand binding assays, all statistical analysis was evaluated with GraphPad Prism using appropriate non-linear regression analyses. Binding data are presented as mean ± SEM. Specific binding data were fitted using non-linear regression and a one-site binding model using the following four-parameter Hill equation Y = Bottom + (Top-Bottom)/(1 + 10^(LogEC50-X)) in GraphPad Prism. Competitive binding experiments were fitted to a one-site binding model and pKi calculated using the K_d value of 34.64 nM determined from the saturation binding. In the ERK1/2 activation assay, the density of phospho ERK1/2 and total ERK1/2 was determined by ImageJ software and density of phospho ERK1/2 was normalized by total ERK1/2. Data for three independent experiments were analysed by the Kruskal-Wallis test followed by Dunn's multiple comparisons test using GraphPad Prism. A non-parametric test was applied because the control data did not meet the criterion for parametric distribution. In the inhibition of forskolin-induced cAMP assay, the cAMP concentrations were calculated using a cAMP standard curve (0.3–750 nM). The data from three experiments were analysed using one-way ANOVA followed by Tukey's (when the mean of each group is compared with means of every other group) or Bonferroni's post hoc (when means of selected groups are compared) test using GraphPad Prism. The concentration-response data were analysed by non-linear fitting and estimation of pEC_{50} in GraphPad Prism.

3. Results

3.1. Modelling and synthesis of the stapled peptides

The root mean square fluctuation (RMSF) is useful for identifying the parts of the peptide that is more or less flexible during the MD simulation and to compare the flexibility of different peptides. In Supplementary Fig. 1, the RMSF averaged is plotted against residue index for the B chain of intact human relaxin-3, the wild type relaxin-3 B chain in isolation, the double mutant of the relaxin-3 B chain in which the Cys residues at positions 10 and 22 were mutated to Ser to prevent cyclization and oligomerization of the peptides, and the two stapled peptides. The isolated relaxin-3 B chains have higher RMSF than the intact human relaxin-3 contain both the A chain and the B chain indicating that the A chain provides some stabilization especially of the central part of the B chain. The 14s18 stapled peptide has similar RMSF as the double mutant and native B chain. The 18s22 stapled peptide has significantly lower RMSF than wild type and double mutant relaxin-3 B chain indicating a rigidifying effect of the staple.

The protein secondary structure elements (SSE) distribution was monitored throughout the simulation. These are α-helixes as no beta strands are present in the B chain of relaxin-3. SSE's were plotted versus residue index and graphs for the chain B of intact human relaxin-3, wild type relaxin-3 B chain, double mutant relaxin-3 B chain and the two stapled peptides are shown in Supplementary Fig. 2. These plots are useful for determining if the stapling stabilizes the helical part of the protein. Intact human relaxin-3 containing both the A chain and the B chain is the structure that is most helical but only slightly more than the native relaxin-3 B chain and double mutant B chain. The 14s18 stapled B chain was a helical peptide

with only the part between the staple maintaining the secondary structure. The 18s22 stapled peptide was predicted to be as helical as the native B chain peptide and in the modelling it was the most rigid of all single chain peptides as indicated by the lowest RMSD.

The stapled peptides were synthesised by substituting the amino acids at i(14) and i+4(18) positions or i(18) and i+4(22) positions of the relaxin-3 B chain with (S)2-(4′-pentenyl)alanine and subsequent RCM (performed by Biosynthesis Inc., USA). The molecular weight and purity of the peptides were analysed by mass spectrometry and RP- HPLC. Mass spectrometry analysis revealed that the observed mass of 18s22 and 14s18 were 3074.19 and 3014.95 respectively. The purity as analysed by RP-HPLC was >97% for 18s22 and >95% for 14s18. The peptide purified using RP-HPLC displayed a single peak with a high purity profile (>95%) product. In many cases, the RCM reaction yields one major olefin isomer, which is often difficult to identify, and in this case, the short (i to i+4) stapling approach in principle avoids the incidence of cis/trans isomerization within the rings. Thus, it is likely that the single RP-HPLC peak represents a predominance of one major olefin isomer. We did not however isolate or identify a specific isomer.

3.2. Conformational analysis of the stapled peptides

Secondary structure of peptides was determined by CD spectroscopy in the far-UV spectral region (190–260 nm). At these wavelengths the chromophore is the peptide bond, and the signal arises when it is located in a regular, folded environment. α-helix, ß-sheet and random coil structures give rise to characteristic CD spectrum. The mean residual molar ellipticity of each secondary structure type in the peptides depicts the characteristic curve of an α-helix for the 14s18, 18s22 stapled peptides whereas the relaxin-3 B chain double mutant has a random coil structure and the intact human relaxin-3 containing both the A chain and B chain has a mixture of α-helix and ß-sheets (Fig. 2A).

CD was employed to determine the mean helical content of the stapled peptides, 14s18 and 18s22, along with the relaxin-3 B chain double mutant as a control unstapled peptide. Differences in $\Theta_{222\,nm}$ indicate change in helical content and can be used to determine a percentage helicity value. We calculated percentage helicity (Table 1) as previously described [39,40]. 14s18 had an enhanced α-helicity profile of 18.5% helical content compared with the 1.80% helical content of the unstapled peptide. 18s22 had also

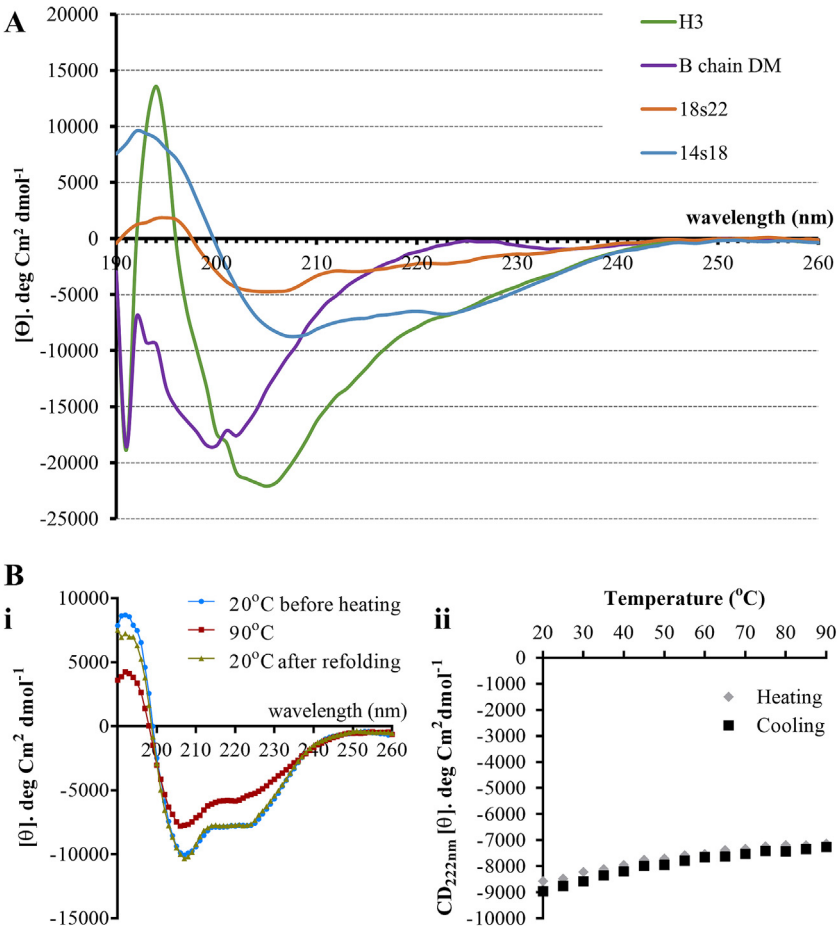

Fig. 2. (A) Circular dichroism (CD) spectra of intact human relaxin-3 (H3; green), the relaxin-3 B chain Cys10Ser+Cys22Ser double mutant (B chain DM; purple), the 18s22 stapled relaxin-3 B chain (18s22; orange) and the 14s18 stapled relaxin-3 B chain (14s18; blue). All compounds were prepared in water with concentration adjusted to 62.5 μM (0.2 mg/ml). H3 is comprised of both the A chain and B chain and the CD spectra reflects a complex mixture of secondary structural conformations. The CD spectra of B chain DM is consistent with this peptide being a relatively unstructured random coil. The CD spectra of 18s22 and 14s18 indicate the presence of α-helicity. (B) Thermodynamic stability of the 14s18 stapled peptide was assessed by variable temperature (VT)-CD spectral analysis. (i) The temperature-dependent CD spectrum was scanned at 5 °C intervals over a temperature range of 20–90 °C at wavelengths from 190 to 260 nm. Data are plotted for 20 °C before heating (blue), at 90 °C (dark red) and after cooling to 20 °C (green). The peptide was dissolved in water with the concentration ranging from 50 to 65 μM. (ii) Changes in CD intensity at 222 nm as a function of temperature. The ellipticity at 222 nm was measured every 5 °C from 20 to 90 °C with a temperature slope of 1 °C/min during heating (black squares) and cooling (grey diamonds) cycles. The spectra plotted are an average of 3 independent scans with a scan speed of 20 nm/min and are expressed as mean residual weight ellipticity. (For interpretation of the references to color in this figure legend, the reader is referred to the web version of this article.)

Table 1
Percentage helicity of non-stapled and stapled relaxin-3 B chain peptides as determined by analysis of circular dichroism (CD).

Peptide	θ_{222} nm	% helicity
B chain DM	−650.5999	1.80
18s22	−2240.0269	6.17
14s18	−6720.0969	18.51

B chain DM: relaxin-3 B chain Cys10Ser + Cys22Ser double mutant; 18s22:18s22 stapled relaxin-3 B chain; 14s18: 14s18 stapled relaxin-3 B chain.

an enhanced the helicity profile albeit much lower than 14s18 with 6.2% helical content.

3.3. Thermal melts as a measure of stability

As the CD spectra data indicated that 14s18 was the most helical of the stapled peptides we selected this peptide for determination of thermal stability by CD analysis. The random coil structure of control relaxin-3 B chain double mutant was not sufficiently helical to generate meaningful thermal stability data by CD analysis. For most peptides, secondary structure is lost upon unfolding and the far-UV CD spectra of a folded and unfolded peptides are distinct. We obtained the thermodynamics of peptide unfolding by (a) collecting the complete spectra (190–260 nm) as a function of temperature and (b) by measuring the intensity of the CD signal at a fixed wavelength (e.g. 222 nm for an α-helical protein) as a function of temperature giving a measure of thermal stability. The full spectra (190–260 nm) of 14s18 at 20 °C shows the ordered structure of an α-helical peptide and the peptide unfolds when it is gradually heated from 20 to 90 °C (Fig. 2Bi). At 90 °C it is partially unfolded as indicated by an upward shift in the CD band, however it regains back its folded conformation when it is cooled down from 90 to 20 °C (Fig. 2Bi), suggesting thermally stable and reversible conformational transition.

We also characterized the unfolding by following the change in ellipticity at 222 nm to determine whether a peptide has unfolding or folding intermediates. As shown in Fig. 2Bii, a linear increase of the ellipticity at 222 nm for 14s18 has been observed for both heating and cooling with a slope of 20.86 ± 1.324 (for heating) and 23.47 ± 1.519 (for cooling) degcm^{2}dmol^{-1} °C^{-1} (Fig. 2Bii). At higher temperatures, the decrease in CD ellipticity indicates that the peptide is partially unfolded and the linear dependency also indicates less energy difference between the two states.

We further used this information to predict the melting transition point [50] for 14s18 stapled peptide during unfolding transition between two states: folded, F, and unfolded, U. T_M of the 14s18 falls near to (50–55 °C) whereas the relaxin-3 B chain double mutant did not have a cooperative melting transition point in this temperature range, and therefore its melting temperature was indeterminable by this method.

3.4. Proteolytic stability assay

In order to compare the proteolytic stability of the 14s18 stapled relaxin-3 B chain with the relaxin-3 B chain double mutant, we incubated equal amounts (μg) of the peptides with endoproteinase Glu-C isolated from *Staphylococcus aureus* V8 that is predicted by the ExPASy Peptide Cutter software to cleave the B chain double mutant at the Glu residue at the 13th position to give two products of 1597 Da and 1432 Da. 14s18 incubated with endoproteinase Glu-C remained intact while the B chain double mutant was digested to produce <2 kDa products (Fig. 3). These data are consistent with the prediction that hydrocarbon stapling stabilizes the relaxin-3 B chain against proteolysis.

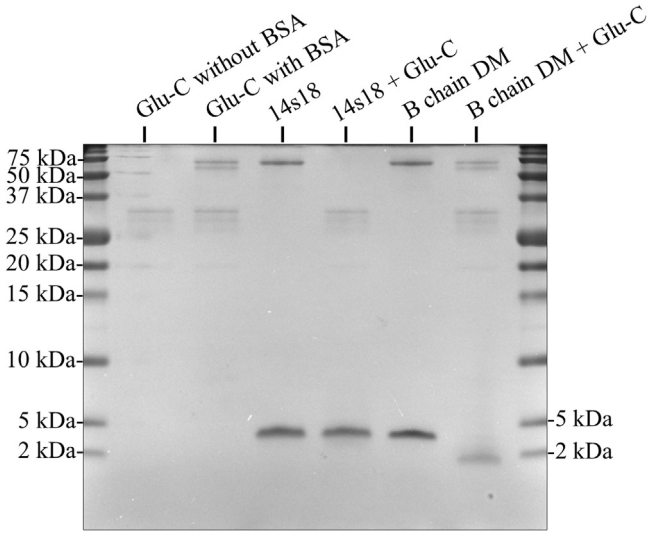

Fig. 3. Hydrocarbon stapling of the B chain of relaxin-3 protects against proteolysis. Coomassie Brilliant Blue R-250 stained tricine SDS-PAGE of endoproteinase Glu-C with and without BSA and 14s18 stapled relaxin-3 B chain (14s18) and relaxin-3 B chain Cys10Ser + Cys22Ser double mutant (B chain DM) with and without Glu-C incubated at 37 °C for 1 h. 14s18 incubated with endoproteinase Glu-C remains intact while the B chain DM is digested to produce <2 kDa products.

3.5. Ligand binding assays

R3 B1-22R has been reported to be a selective RXFP3 ligand [30]. We had applied a site-directed synthesis strategy to chelate Eu-DTPA to the N-terminus of single chain R3 B1-22R. Assays using Eu-chelate-peptides have been reported to be highly reproducible, showed excellent signal-to-noise ratios and were faster than radioisotope-based assays and in other cases DTPA labelling of bioactive peptide has been described [51–53]. The pharmacological profile of Eu-DTPA-R3 B1-22R was characterized by both saturation and competition binding assays.

3.5.1. Saturation binding assay

To test whether Eu-DTPA-R3 B1-22R had receptor binding activity, we first carried out a saturation binding assay using HEK293T cells stably expressing RXFP3 (HEK-RXFP3) (Fig. 4A). To determine the total binding, cells were incubated with different concentrations of Eu-DTPA-R3 B1-22R in a 96 well plate, and to measure the non-specific binding 1 μM of unlabelled R3 B1-22R was used. The non-specific binding was found to be substantially less than total binding at all concentration of Eu-DTPA-R3 B1-22R tested (Fig. 4B). Eu-DTPA-R3 B1-22R binds in a specific and saturable manner and fitted best to a one-site binding model in the hyperbolic ligand binding function $Y = B_{max}X/(Kd + X)$ (Fig. 4C). The calculated dissociation constant (K_d) for Eu-DTPA-R3 B1-22R was 34.64 ± 3.83 (n = 3) and the maximal binding (B_{max}) was 1061 (fmol/mg) ± 46.68 (n = 3) as shown in Fig. 4C, suggesting that Eu-DTPA-labelled peptide still has binding affinity for RXFP3 despite the presence of the large DTPA/Eu^{+3} moiety. The Scatchard plot of the specific binding data was linear (Fig. 4C inset), which is consistent with one-site binding of Eu-DTPA-R3 B1-22R with the receptor, RXFP3. The calculated K_d and B_{max} values are slightly different with the previous ligand binding studies done in CHO-RXFP3 cell lines [54].

3.6. Competition binding of stapled peptides

Once the Eu-DTPA-R3 B1-22R was characterized by the saturation binding experiments described above and determined to retain binding affinity for RXFP3, we used the labelled ligand as a tracer

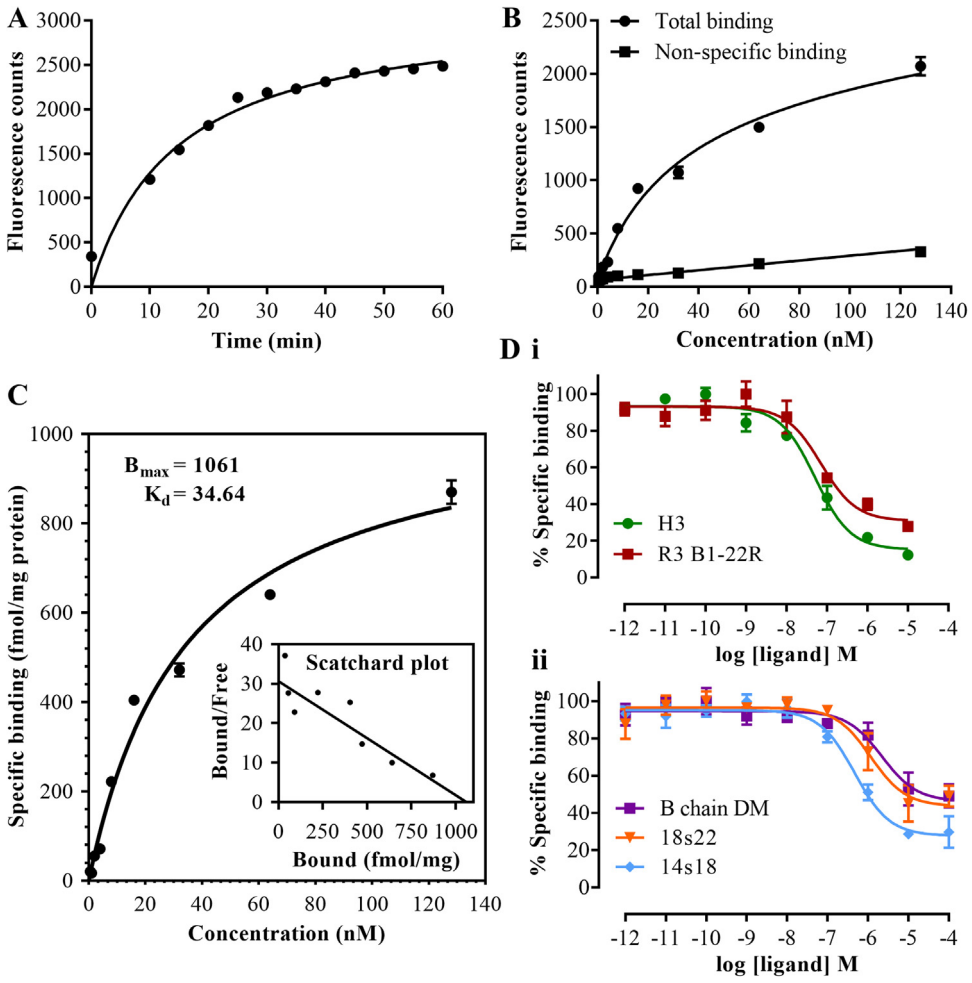

Fig. 4. (A) Determination of the time course of europium (Eu) release from Eu-diethylenetriaminepentaacetic acid (DTPA)-R3 B1-22R. 10 μl of 10 nM Eu-DTPA-R3 B1-22R was mixed with dissociation-enhanced lanthanide fluorescent immunoassay (DELFIA) enhancement solution in triplicates and the fluorescence was measured at 5 min intervals for 60 min. The signal approached a maximum of approximately 2200 fluorescent counts at 30 min. (B) Characterization of binding of Eu-DTPA-R3 B1-22R to RXFP3 in HEK293T cells stably expressing RXFP3 (HEK-RXFP3). Total binding (circles) was determined for increasing concentrations (range 0.5–128 nM) of Eu-DTPA-R3 B1-22R alone while non-specific binding (squares) was determined for the same range of concentration of Eu-DTPA-R3 B1-22R in the presence of 1 μM unlabelled R3 B1-22R. The measured fluorescence counts were expressed as mean ± SEM (n = 3) of triplicate determinations from three independent experiments. (C) K_d and B_{max} were determined by fitting a one-binding site model to the specific binding of Eu-DTPA-R3 B1-22R. Specific binding data were fitted to $Y = B_{max}.X/(K_d + X)$. The K_d and B_{max} value were determined to be 34.64 ± 3.83 SEM (n = 3) and 1061 ± 46.68 SEM (fmol/mg protein) (n = 3), respectively. A representative Scatchard plot (inset) shows a linear relationship between the bound/free ratio and bound ligand, confirming a one-site binding model for the binding of Eu-DTPA-R3 B1-22R with RXFP3. Data are presented as mean ± SEM of triplicates from three independent experiments. (D) Competition binding curves for relaxin-3 analogues in HEK-RXFP3 cells using Eu-DTPA-R3 B1-22R as the labelled ligand. Various concentrations of (i) intact human relaxin-3 (1 pM to 10 μM H3; green circles) and unlabelled R3 B1-22R (1 pM to 10 μM R3 B1-22R; dark red) and (ii) the relaxin-3 B chain Cys10Ser + Cys22Ser double mutant (1 pM to 100 μM B chain DM; purple), the 18s22 stapled relaxin-3 B chain (1 pM to 100 μM 18s22; orange) and the 14s18 stapled relaxin-3 B chain (1 pM to 100 μM 14s18; blue) were added to cells to compete for RXFP3 binding with 8 nM of Eu-DTPA-R3 B1-22R labelled ligand. Data are presented as mean ± SEM of triplicates from three to four independent experiments. The error bar is not shown for data points where the error bar is shorter than the height of the symbol. (For interpretation of the references to color in this figure legend, the reader is referred to the web version of this article.)

in competition binding assays (Fig. 4D) to study the interaction of these receptors with their ligands. To rule out any significant difference in agonist and antagonist binding modes, we first studied the competition binding using various concentrations (1 pM to 10 μM) of unlabelled R3 B1-22R peptide and intact human relaxin-3 (Fig. 4Di). R3 B1-22R demonstrated a pK_i of 7.24 ± 0.17 (n = 3), which is not significantly different from intact human relaxin-3 with a pK_i of 7.38 ± 0.11 (n = 3) ($p > 0.05$ by one-way ANOVA and Tukey's post hoc comparison; Table 2). In the similar manner, we carried out the competition binding assay using various concentrations (1 pM to 100 μM) of the stapled peptides (14s18 and 18s22) and the relaxin-3 B chain double mutant (Fig. 4Dii). The calculated pK_i values demonstrated a higher binding affinity for the 14s18 stapled peptide ($pK_i = 6.42 \pm 0.13$) as compared to the relaxin-3 B chain double mutant peptide ($pK_i = 5.75 \pm 0.24$). The 18s22 stapled peptide had an intermediate binding affinity ($pK_i = 6.02 \pm 0.23$) between that of the relaxin-3 B chain double mutant peptide and the 14s18 stapled peptide.

3.7. *Intact human relaxin-3 mediated ERK1/2 activation can be detected by an optimized ERK1/2 activation assay*

Quantification of the data revealed that the peak of ERK1/2 activation can be detected 8–10 min post stimulation with 10 nM intact human relaxin-3 in HEK-RXFP3 (Fig. 5A and B) and CHO-RXFP3 (Fig. 5C and D) cell lines by this method. However, ERK1/2 activation was observed neither in HEK293T (Fig. 5E) nor in CHO-K1 (Fig. 5F) cells with 10 nM intact human relaxin-3 at similar time points.

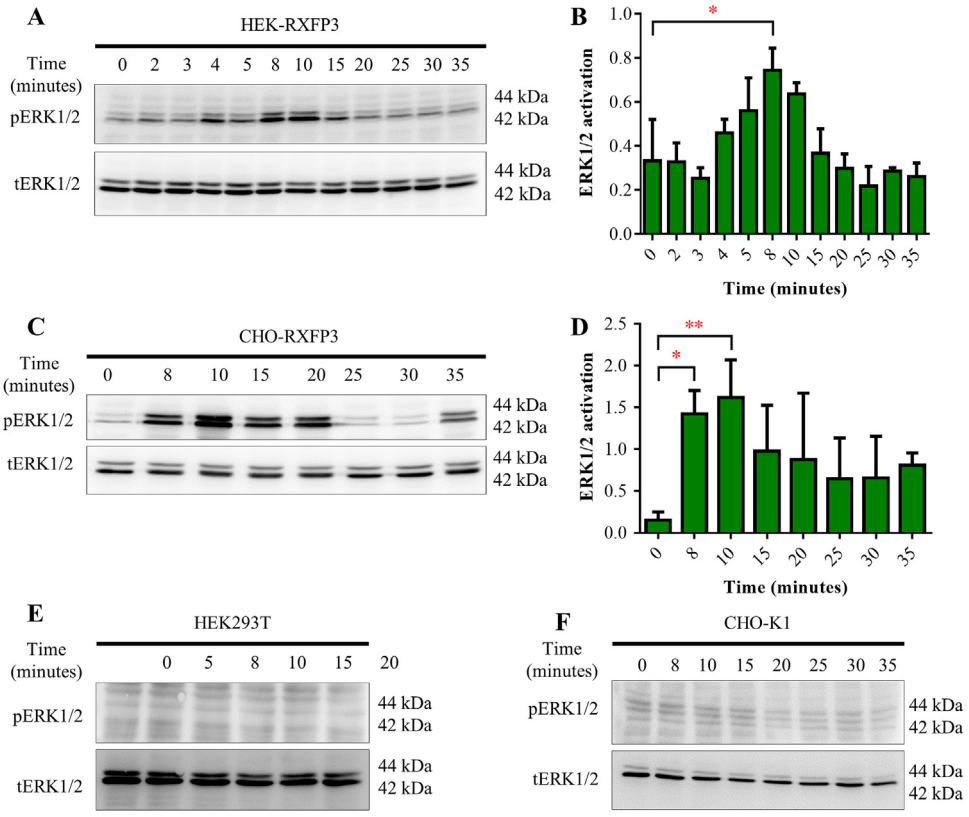

Fig. 5. The time course of ERK1/2 activation by 10 nM intact human relaxin-3 (H3) in (A) HEK-RXFP3 cells with (B) quantified relative density presented as activation of ERK1/2, (C) CHO-RXFP3 cells with (D) quantified relative density presented as activation of ERK1/2, (E) wild type HEK293T cells, and (F) wild type CHO-K1 cells. In (B) and (D) the quantified relative density activation of ERK1/2 is represented as mean ± SEM (n = 3). Statistical analysis by one-way ANOVA followed by Dunnett's post hoc test corrected for multiple comparisons: $^{*}p < 0.05$, $^{**}p < 0.01$.

Table 2
Measures of binding affinity and potency at RXFP3 receptors.

RXFP3 ligand	Eu-DTPA-R3 B1-22R pK_i	RXFP3 cAMP pEC_{50}
H3	7.38 ± 0.11	9.49 ± 0.14
R3 B1-22R	7.24 ± 0.17	n.d.
B chain DM	5.75 ± 0.24	6.61 ± 0.24
18s22	6.02 ± 0.23	n.d.
14s18	6.42 ± 0.13	7.47 ± 0.16

Data are presented as the mean ± SEM (n = 3–4) of triplicates from three to four independent experiments. H3: intact human rleaxin-3; B chain DM: relaxin-3 B chain Cys10Ser + Cys22Ser double mutant; 18s22:18s22 stapled relaxin-3 B chain; 14s18: 14s18 stapled relaxin-3 B chain; n.d., not determined.

3.8. Intact human relaxin-3 mediated inhibition of cAMP accumulation by RXFP3 can be detected by the inhibition of forskolin-induced cAMP assay

Activation of adenylate cyclase by forskolin and inhibition of adenylate cyclase by $G_{\alpha i}$ has been reported before [55,56]. An inhibition of forskolin-induced cAMP assay revealed that, 10 nM intact human relaxin-3 is able to significantly reduce the forskolin- (5 μM) induced cAMP levels in HEK-RXFP3 (Fig. 6A) and CHO-RXFP3 (Fig. 6C) cells as reported in previous publications [15]. However, in wild type HEK293T (Fig. 6B) and CHO-K1 (Fig. 6D) cells, 10 nM intact human relaxin-3 was not able to significantly reduce the forskolin- (5 μM) induced cAMP levels. Meanwhile, in the SN56 neuronal-like cell line, which expresses RXFP3, 100 nM intact human relaxin-3 was able to significantly reduce forskolin- (3 μM) induced cAMP (Fig. 6E).

3.9. Stapled B chains of relaxin-3 activate ERK1/2 in HEK-RXFP3 cells

The 18s22 stapled B chain of relaxin-3 was able to significantly activate ERK1/2 compared to the vehicle at a 10 μM concentration (Fig. 7C). However, 18s22 did not significantly activate ERK1/2 at 100 nM and 1 μM (Fig. 7A and B) although the statistical analysis did not show a significant difference in the ERK1/2 activation between the intact human relaxin-3 (10 nM) and the 100 nM and 1 μM 18s22 treatments (Fig. 7A and B). The 14s18 stapled B chain of relaxin-3 significantly activated ERK1/2 at 10 μM compared to the intact human relaxin-3 (10 nM) treatment (Fig. 7F) but not at 100 nM or 1 μM (Fig. 7D and E).

3.10. Stapled relaxin-3 B chain peptides inhibit cAMP a cells

18s22 stapled relaxin-3 B chain significantly inhibited the forskolin (5 μM) induced cAMP levels at all the concentrations tested (100 nM, 1 μM and 10 μM) compared to the vehicle treatment but did not show a clear dose-dependent effect (Fig. 8A–C). Progressive reduction in the cAMP concentration was observed with increasing stapled peptide concentrations. However, 14s18 stapled relaxin-3 B chain showed progressive, dose-dependent reduction in the forskolin-induced cAMP levels significant from 1 μM onwards (Fig. 8E and F) while 100 nM 14s18 was not sufficient to significantly inhibit the forskolin-induced cAMP levels (Fig. 8D). As the 14s18 stapled peptide had shown the greatest tendency towards a clear dose-dependent effect, we selected this peptide for further analysis of the concentration-response relationship with inhibition of forskolin-induced cAMP levels. Intact human

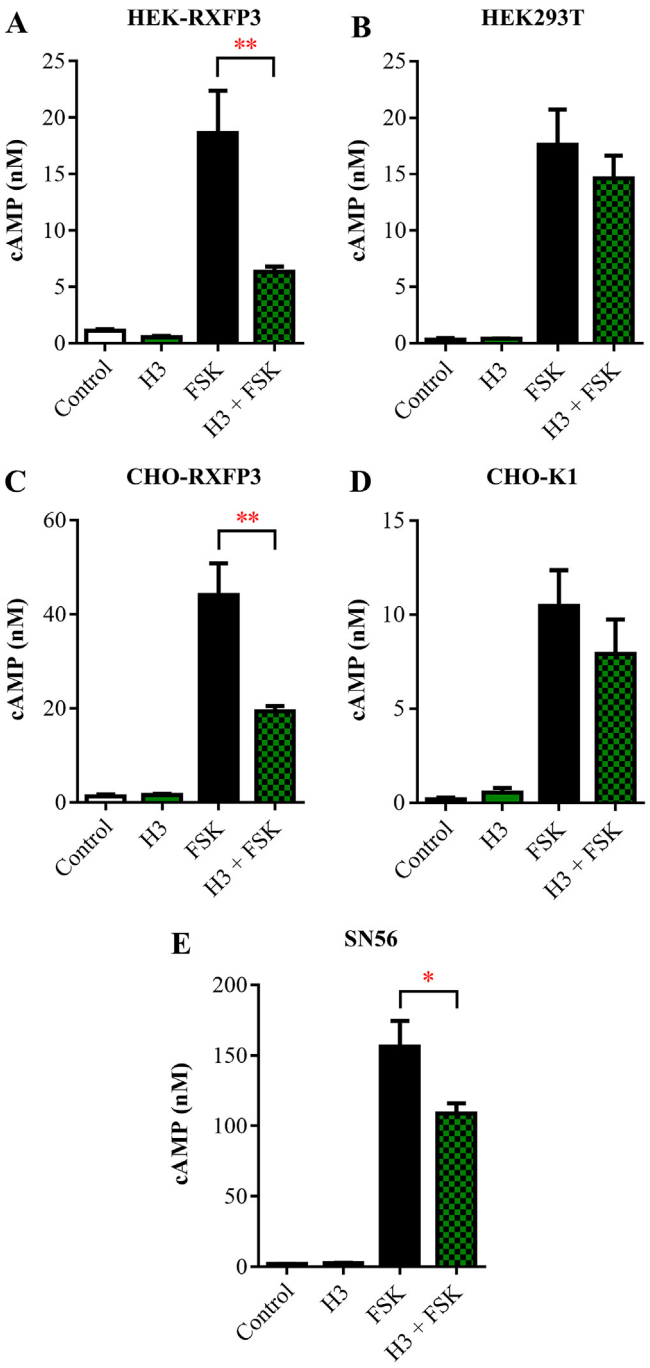

Fig. 6. Inhibition of forskolin (FSK) induced cAMP assay by (A) 10 nM H3 relaxin (H3) in HEK-RXFP3 cells (B) 10 nM H3 relaxin in HEK293T cells (C) 10 nM H3 relaxin CHO-RXFP3 cells (D) 10 nM H3 relaxin in CHO-K1 cells and (E) 100 nM H3 relaxin in SN56 cells. cAMP concentration in nM represented as mean ± SEM (n = 3). Statistical analysis by one-way ANOVA followed by Tukey's post hoc test corrected for multiple comparisons: *p < 0.05, **p < 0.01, ***p < 0.001.

relaxin-3 dose-dependently inhibited forskolin-induced cAMP levels with a pEC_{50} of 9.49 ± 0.14 in HEK-RXFP3 cells (Table 2) but have no significant dose-dependent effect on forskolin-induced cAMP levels in wild type HEK293T cells (Fig. 8G). The relaxin-3 B chain double mutant was significantly less potent with a pEC_{50} of 6.61 ± 0.24 in HEK-RXFP3 cells (Fig. 8H; Table 2). The 14s18 stapled peptide was significantly more potent ($p < 0.05$, one-way ANOVA followed by Bonferroni multiple comparison's test) than the relaxin-3 B chain double mutant with a pEC_{50} of 7.47 ± 0.16 in the HEK-RXFP3 cells (Table 2) but had no significant dose-dependent effect on forskolin-induced cAMP levels in wild type HEK293T cells (Fig. 8I).

4. Discussion

In this study, for the first time, we report that stapling of the human relaxin-3 B chain at positions 18, 22 (18s22 stapled peptide) and 14, 18 (14s18 stapled peptide) is able to retain biological activity of the peptide.

In silico modelling had predicted that the 18s22 and 14s18 stapled peptides would be feasible stapled peptides but that the 18s22 stapled peptide would be likely to be more rigid and helical. On synthesis of the stapled peptides and determination of helicity by analysis of CD spectra both 18s22 and 14s18 proved to have α-helical secondary structure but the CD analysis suggested that

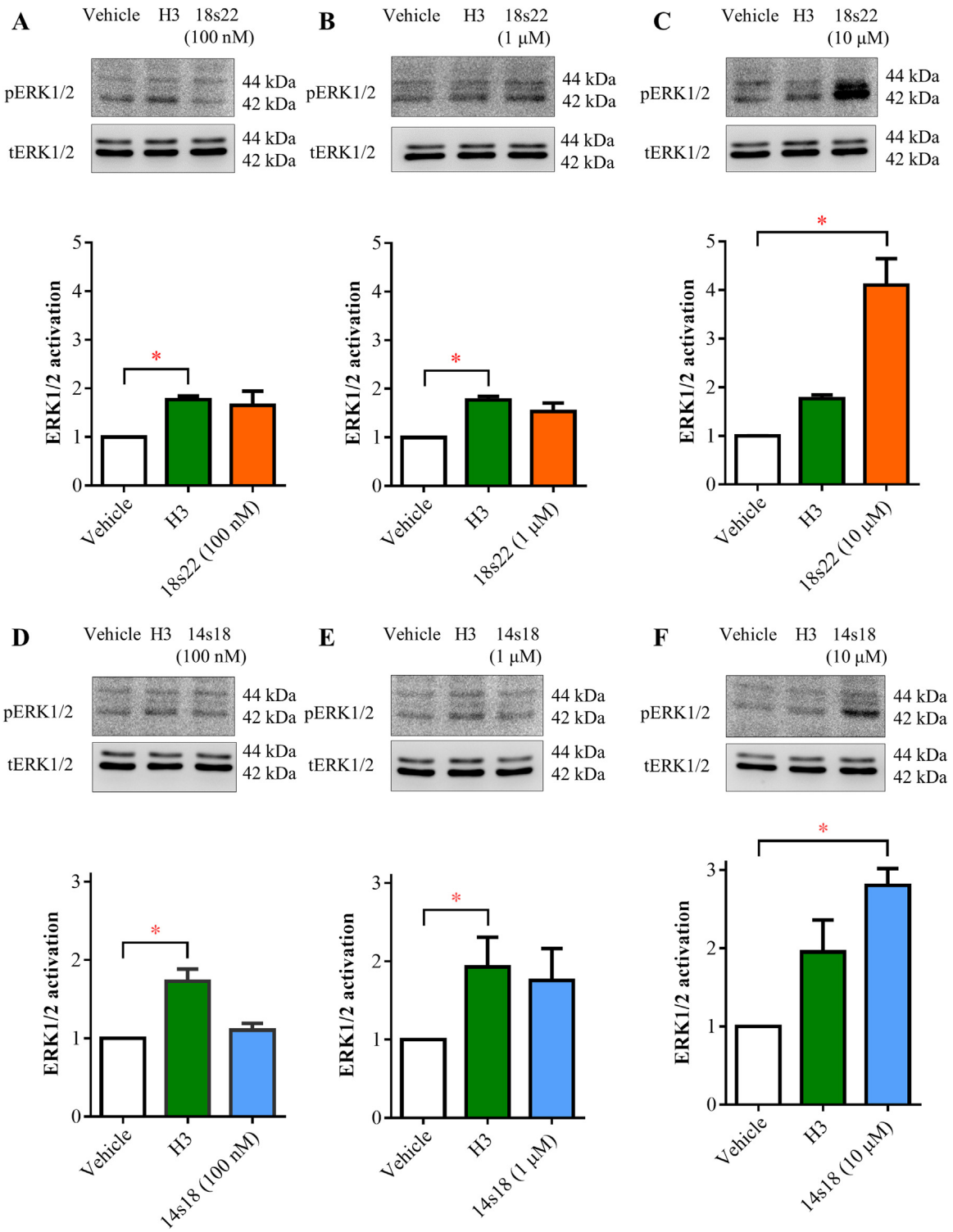

Fig. 7. ERK1/2 activation in HEK-RXFP3 by (A) 100 nM 18s22, (B) 1 μM 18s22, (C) 10 μM 18s22, (D) 100 nM 14s18, (E) 1 μM 14s18 and (F) 10 μM 14s18. Quantified relative density is represented as mean ± SEM (n = 3). Statistical analysis by Kruskal-Wallis test followed by Dunn's multiple comparison test: *p < 0.05.

14s18 was more helical. Because i to i+4 stapling holds the 3.6 residues per turn of an α-helix, it may be that stapling at a more central position in the potentially helical domain of the relaxin-3 B chain in the 14s18 stapled peptide stabilizes the helix best. CD thermal stability analysis demonstrated that 14s18 was able to unfold and refold without losing the helical structure on refolding. These data are consistent with the hypothesis that hydrocarbon stapling of the relaxin-3 B chain may stabilise the peptide in an α-helical conformation much like the A chain disulphide bonds in human relaxin-3. Although hydrocarbon stapling stabilised the α-helical secondary structure of the peptide, certain residues can induce helicity without the formation of a staple. In particular, substitution with α,α amino acids, such as 2-aminoisobutyric acid (Aib), is reported to increase helicity [57–60]. A major difference between use of α,α amino acids without stapling and stapling is that a staple may impart more rigidity. It would interesting in

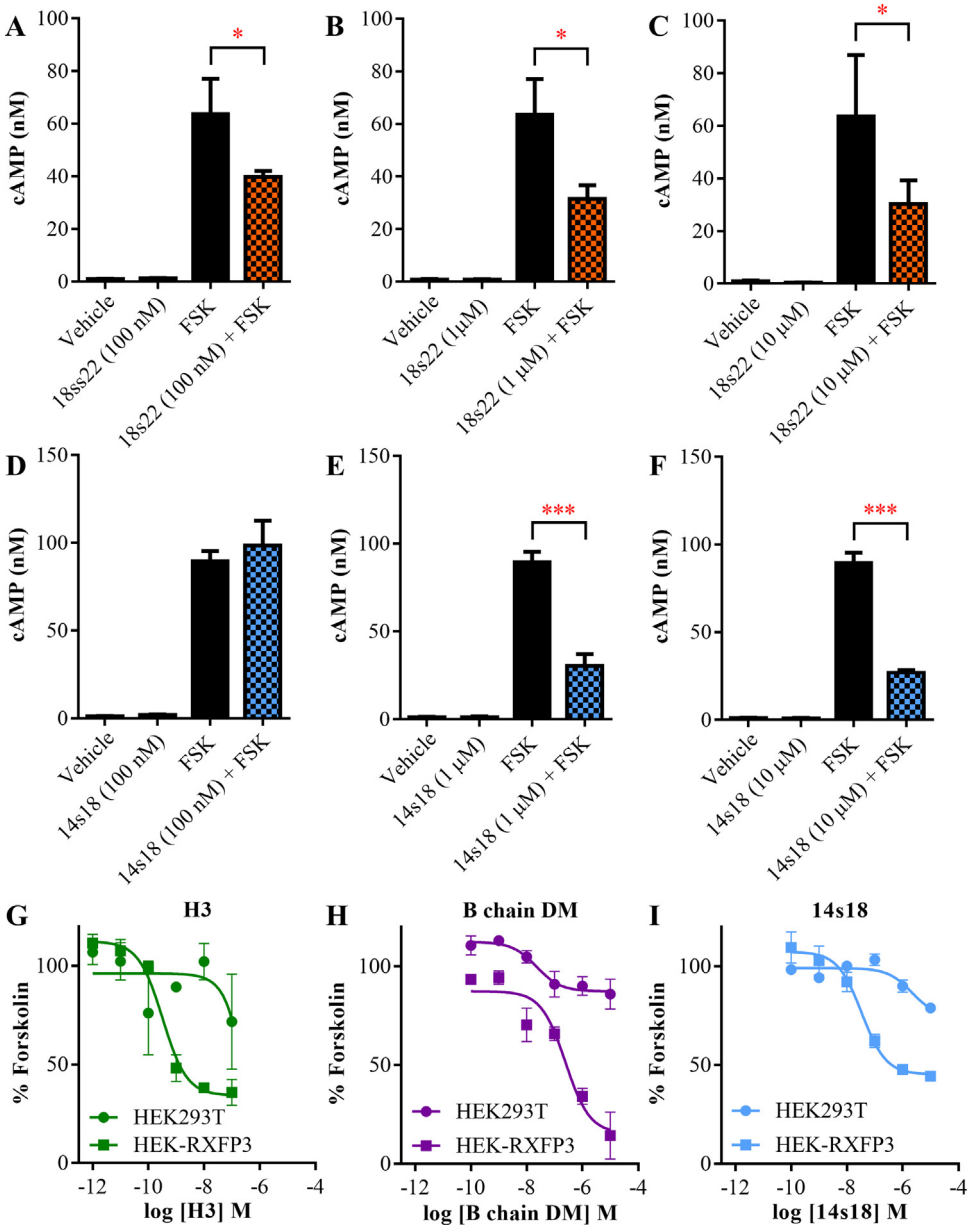

Fig. 8. Inhibition of forskolin (FSK) induced cAMP assay in HEK-RXFP3 cells by (A) 100 nM 18s22 (B) 1 μM 18s22 (C) 10 μM 18s22 (D) 100 nM 14s18 (E) 1 μM 14s18 and (F) 10 μM 14s18. cAMP concentration in nM represented as mean ± SEM (n = 3). (A)–(F) statistical analysis by one-way ANOVA followed by Bonferroni post hoc test: $^{*}p < 0.05$, $^{***}p < 0.001$. Inhibition of forskolin (FSK) induced cAMP in HEK-RXFP3 cells (squares) and HEK293T cells (circles) by (G) 1 pM to 100 nM intact human relaxin-3 (H3); (I) 100 pM to 10 μM relaxin-3 B chain Cys10Ser + Cys22Ser double mutant (B chain DM); and (H) 100 pM to 10 μM 14s18 stapled relaxin-3 B chain (14s18). cAMP concentration is represented as percentage of the forskolin-induced response (mean ± SEM; n = 3). Curves were fit using a four-parameter Hill equation: Y = Bottom + (Top-Bottom)/(1 + 10^(logEC50-X)).

future experiments to explore the correlations of helicity and rigidity with function of relaxin-3 peptides. A proteolytic digestion assay confirmed that hydrocarbon stapling of the B chain increases proteolytic stability of the peptide.

Both 18s22 and 14s18 stapled relaxin-3 B chain peptides bound to RXFP3 receptors with greater affinity than the corresponding unstapled relaxin-3 B chain double mutant control peptide. However, the 14s18 stapled relaxin-3 B chain was more potent. It may be that the greater helicity of the 14s18 stapled relaxin-3 B chain confers greater RXFP3 binding.

Relaxin-3-mediated RXFP3 activation leads to $G_{\alpha i/o}$ coupling to RXFP3 which results in ERK1/2 activation [15] and adenylate cyclase inhibition [6,15]. In order to determine the biological activity of the stapled B chains of relaxin-3, we optimized a Western blot based ERK1/2 activation assay and an ELISA based inhibition of forskolin-induced cAMP assay. Initially, we tested the reproducibility of the assays on few cell lines that overexpress or endogenously express RXFP3, using the cognate ligand H3 relaxin. Results of these assays confirmed that relaxin-3 at 10 nM is able to significantly activate RXFP3 in HEK-RXFP3 and CHO-RXFP3 cells. In the inhibition of forskolin-induced cAMP assay, 10 nM H3 relaxin-3 was able to inhibit adenylate cyclase activity, which could not be overcome by 5 μM forskolin in HEK-RXFP3 and CHO-RXFP3 cells. Further testing of the assays on wild type HEK293T and CHO-K1 cells confirmed the specificity of the response to RXFP3 indicating that this assay can be used to detect $G_{\alpha i/o}$ mediated cAMP inhibition related signalling events in the cell lines tested. In SN56 cells, adenylate

cyclase inhibition was observed at 100 nM relaxin-3 which could not be overcome by 3 μM forskolin.

We sought to determine the ERK1/2 activation in both HEK-RXFP3 and CHO-RXFP3 cell lines, to confirm whether the 8–10 min time point which is different to that reported in previous publications [15] is accurate, and to assess the robustness of the assay. We observed that both cell lines show a peak ERK1/2 activation between 8 and 10 min. Further testing the assays on wild type HEK293T and CHO-K1 cells confirmed the specificity of the response to RXFP3.

We tested the stapled peptides for their ability to activate RXFP3 in HEK-RXFP3 cells. 18s22 stapled B chain of relaxin-3 was able to significantly activate ERK1/2 in HEK-RXFP3 cells at 10 μM. Similar observation was made with 14s18 stapled B chain of relaxin-3, where significant ERK1/2 activation was observed with 10 μM peptide. Moreover, there is an increasing trend of ERK1/2 activation from 100 nM to 10 μM for the 14s18 stapled peptide.

In the inhibition of forskolin-induced cAMP assay, 18s22 stapled B chain of relaxin-3 was able to activate RXFP3 at the concentrations tested (100 nM, 1 μM and 10 μM), but 14s18 stapled B chain of relaxin-3 was able to significantly activate RXFP3 only at 1 μM and 10 μM concentrations. The 14s18 stapled relaxin-3 B chain peptide dose-dependently inhibited forskolin-induced cAMP levels with greater potency than the corresponding unstapled relaxin-3 B chain double mutant control peptide.

The α-helix is a common secondary structure found in peptides. Stapling of α-helices in peptides is the basis of developing stapled peptides which is carried out mostly by hydrocarbon stapling. This technique was first reported by Verdine and co-workers and was used in developing BID BH3 peptides targeting the BCL-2 family proteins [61]. These studies suggest that stapling of peptides render them to be highly stable with increased helicity and affinity. The proteolytic stability of peptides and the blood brain barrier permeability of peptide drugs limiting their usage in targeting CNS disorders. Hydrocarbon stapling or modifications of stapling chemistries may increase proteolytic stability of peptides and enhance their ability to cross biological membranes and the blood brain barrier. The relaxin-3 B chain loses its helicity in the absence of the A chain. Thus, stable analogues of relaxin-3 B chain will be useful tools in understanding its physiological significance. Given that relaxin-3 B chain possesses an α-helix, it is amenable for stapling. Therefore, we designed, synthesised and tested stapled B chains of relaxin-3 to assess their biological activity.

In conclusion, stapling of the B chain of relaxin-3 at 18 and 22 positions and 14 and 18 positions retain their ability to activate RXFP3 with regard to signalling events activated by RXFP3 activation such as $G_{\alpha i/o}$ coupling and ERK1/2 activation. Thus, stapling of the B chain of relaxin-3 is a promising method of developing stable agonists and antagonists of RXFP3 in order to overcome limitations of using existing peptide agonists and antagonists in current relaxin-3/RXFP3 research.

Conflicts of interest

None.

Acknowledgements

This work was supported by the Biomedical Research Council of Singapore (BMRC10/1/21/19/645), the National Medical Research Council of Singapore (NMRC/1287/2011) and the Ministry of Education, Singapore, Academic Research Fund Tier 1 Seed Fund for Basic Science Research (T1-BSRG 2014-03 "Stapled relaxin-3 B chain peptides as novel RXFP3 agonists and antagonists"). We thank Mr. Ho Woon Fei for excellent technical and administrative assistance.

Appendix A. Supplementary data

Supplementary data associated with this article can be found, in the online version, at http://dx.doi.org/10.1016/j.peptides.2016.08.001.

References

[1] R.A. Bathgate, C.S. Samuel, T.C. Burazin, S. Layfield, A.A. Claasz, I.G. Reytomas, N.F. Dawson, C. Zhao, C. Bond, R.J. Summers, L.J. Parry, J.D. Wade, G.W. Tregear, Human relaxin gene 3 (H3) and the equivalent mouse relaxin (M3) gene. Novel members of the relaxin peptide family, J. Biol. Chem. 277 (2) (2002) 1148–1157.
[2] T.N. Wilkinson, T.P. Speed, G.W. Tregear, R.A. Bathgate, Evolution of the relaxin-like peptide family, BMC Evol. Biol. 5 (2005) 14.
[3] F. Shabanpoor, F. Separovic, J.D. Wade, The human insulin superfamily of polypeptide hormones, Vitam. Horm. 80 (2009) 1–31.
[4] M.A. Hossain, K.J. Rosengren, L.M. Haugaard-Jonsson, S. Zhang, S. Layfield, T. Ferraro, N.L. Daly, G.W. Tregear, J.D. Wade, R.A. Bathgate, The A-chain of human relaxin family peptides has distinct roles in the binding and activation of the different relaxin family peptide receptors, J. Biol. Chem. 283 (25) (2008) 17287–17297.
[5] R.A. Bathgate, F. Lin, N.F. Hanson, L. Otvos Jr., A. Guidolin, C. Giannakis, S. Bastiras, S.L. Layfield, T. Ferraro, S. Ma, C. Zhao, A.L. Gundlach, C.S. Samuel, G.W. Tregear, J.D. Wade, Relaxin-3: improved synthesis strategy and demonstration of its high-affinity interaction with the relaxin receptor LGR7 both in vitro and in vivo, Biochemistry 45 (3) (2006) 1043–1053.
[6] C. Liu, E. Eriste, S. Sutton, J. Chen, B. Roland, C. Kuei, N. Farmer, H. Jornvall, R. Sillard, T.W. Lovenberg, Identification of relaxin-3/INSL7 as an endogenous ligand for the orphan G-protein-coupled receptor GPCR135, J. Biol. Chem. 278 (50) (2003) 50754–50764.
[7] T.C. Burazin, R.A. Bathgate, M. Macris, S. Layfield, A.L. Gundlach, G.W. Tregear, Restricted, but abundant, expression of the novel rat gene-3 (R3) relaxin in the dorsal tegmental region of brain, J. Neurochem. 82 (6) (2002) 1553–1557.
[8] S. Ma, P.J. Shen, Q. Sang, J.L. Lanciego, A.L. Gundlach, Distribution of relaxin-3 mRNA and immunoreactivity and RXFP3-binding sites in the brain of the macaque, Macaca fascicularis, Ann. N. Y. Acad. Sci. 1160 (2009) 256–258.
[9] M. Goto, L.W. Swanson, N.S. Canteras, Connections of the nucleus incertus, J. Comp. Neurol. 438 (1) (2001) 86–122.
[10] S. Ma, P. Bonaventure, T. Ferraro, P.J. Shen, T.C. Burazin, R.A. Bathgate, C. Liu, G.W. Tregear, S.W. Sutton, A.L. Gundlach, Relaxin-3 in GABA projection neurons of nucleus incertus suggests widespread influence on forebrain circuits via G-protein-coupled receptor-135 in the rat, Neuroscience 144 (1) (2007) 165–190.
[11] F.E. Olucha-Bordonau, V. Teruel, J. Barcia-Gonzalez, A. Ruiz-Torner, A.A. Valverde-Navarro, F. Martinez-Soriano, Cytoarchitecture and efferent projections of the nucleus incertus of the rat, J. Comp. Neurol. 464 (1) (2003) 62–97.
[12] V. Teruel-Marti, A. Cervera-Ferri, A. Nunez, A.A. Valverde-Navarro, F.E. Olucha-Bordonau, A. Ruiz-Torner, Anatomical evidence for a ponto-septal pathway via the nucleus incertus in the rat, Brain Res. 1218 (2008) 87–96.
[13] K. Boels, I. Hermans-Borgmeyer, H.C. Schaller, Identification of a mouse orthologue of the G-protein-coupled receptor SALPR and its expression in adult mouse brain and during development, Dev. Brain Res. 152 (2) (2004) 265–268.
[14] R.A. Bathgate, R. Ivell, B.M. Sanborn, O.D. Sherwood, R.J. Summers, International Union of Pharmacology LVII: recommendations for the nomenclature of receptors for relaxin family peptides, Pharmacol. Rev. 58 (1) (2006) 7–31.
[15] E.T. van der Westhuizen, T.D. Werry, P.M. Sexton, R.J. Summers, The relaxin family peptide receptor 3 activates extracellular signal-regulated kinase 1/2 through a protein kinase C-dependent mechanism, Mol. Pharmacol. 71 (6) (2007) 1618–1629.
[16] E.T. Van der Westhuizen, P.M. Sexton, R.A. Bathgate, R.J. Summers, Responses of GPCR135 to human gene 3 (H3) relaxin in CHO-K1 cells determined by microphysiometry, Ann. N. Y. Acad. Sci. 1041 (2005) 332–337.
[17] J. Chen, C. Kuei, S.W. Sutton, P. Bonaventure, D. Nepomuceno, E. Eriste, R. Sillard, T.W. Lovenberg, C. Liu, Pharmacological characterization of relaxin-3/INSL7 receptors GPCR135 and GPCR142 from different mammalian species, J. Pharmacol. Exp. Ther. 312 (1) (2005) 83–95.
[18] A. Banerjee, P.J. Shen, S. Ma, R.A. Bathgate, A.L. Gundlach, Swim stress excitation of nucleus incertus and rapid induction of relaxin-3 expression via CRF1 activation, Neuropharmacology 58 (1) (2010) 145–155.
[19] Y. Watanabe, Y. Miyamoto, T. Matsuda, M. Tanaka, Relaxin-3/INSL7 regulates the stress-response system in the rat hypothalamus, J. Mol. Neurosci.: MN 43 (2) (2011) 169–174.
[20] B.M. McGowan, S.A. Stanley, K.L. Smith, N.E. White, M.M. Connolly, E.L. Thompson, J.V. Gardiner, K.G. Murphy, M.A. Ghatei, S.R. Bloom, Central relaxin-3 administration causes hyperphagia in male Wistar rats, Endocrinology 146 (8) (2005) 3295–3300.
[21] B.M. McGowan, S.A. Stanley, K.L. Smith, J.S. Minnion, J. Donovan, E.L. Thompson, M. Patterson, M.M. Connolly, C.R. Abbott, C.J. Small, J.V. Gardiner,

M.A. Ghatei, S.R. Bloom, Effects of acute and chronic relaxin-3 on food intake and energy expenditure in rats, Regul. Pept. 136 (1–3) (2006) 72–77.
[22] S.W. Sutton, J. Shelton, C. Smith, J. Williams, S. Yun, T. Motley, C. Kuei, P. Bonaventure, A. Gundlach, C. Liu, T. Lovenberg, Metabolic and neuroendocrine responses to RXFP3 modulation in the central nervous system, Ann. N. Y. Acad. Sci. 1160 (2009) 242–249.
[23] C. Lenglos, A. Mitra, G. Guevremont, E. Timofeeva, Regulation of expression of relaxin-3 and its receptor RXFP3 in the brain of diet-induced obese rats, Neuropeptides 48 (3) (2014) 119–132.
[24] J. Munro, O. Skrobot, M. Sanyoura, V. Kay, M.T. Susce, P.E. Glaser, J. de Leon, A.I. Blakemore, M.J. Arranz, Relaxin polymorphisms associated with metabolic disturbance in patients treated with antipsychotics, J. Psychopharmacol. 26 (3) (2012) 374–379.
[25] H. Yamamoto, H. Shimokawa, T. Haga, Y. Fukui, K. Iguchi, K. Unno, M. Hoshino, A. Takeda, The expression of relaxin-3 in adipose tissue and its effects on adipogenesis, Protein Pept. Lett. 21 (6) (2014) 517–522.
[26] S. Ma, F.E. Olucha-Bordonau, M.A. Hossain, F. Lin, C. Kuei, C. Liu, J.D. Wade, S.W. Sutton, A. Nunez, A.L. Gundlach, Modulation of hippocampal theta oscillations and spatial memory by relaxin-3 neurons of the nucleus incertus, Learn. Mem. 16 (11) (2009) 730–742.
[27] S. Ma, A. Blasiak, F.E. Olucha-Bordonau, A.J. Verberne, A.L. Gundlach, Heterogeneous responses of nucleus incertus neurons to corticotrophin-releasing factor and coherent activity with hippocampal theta rhythm in the rat, J. Physiol. 591 (Pt. 16) (2013) 3981–4001.
[28] L. Alvarez-Jaimes, S.W. Sutton, D. Nepomuceno, S.T. Motley, M. Cik, E. Stocking, J. Shoblock, P. Bonaventure, In vitro pharmacological characterization of RXFP3 allosterism: an example of probe dependency, PLoS One 7 (2) (2012) e30792.
[29] F. Shabanpoor, M. Akhter Hossain, P.J. Ryan, A. Belgi, S. Layfield, M. Kocan, S. Zhang, C.S. Samuel, A.L. Gundlach, R.A. Bathgate, F. Separovic, J.D. Wade, Minimization of human relaxin-3 leading to high-affinity analogues with increased selectivity for relaxin-family peptide 3 receptor (RXFP3) over RXFP1, J. Med. Chem. 55 (4) (2012) 1671–1681.
[30] L.M. Haugaard-Kedstrom, F. Shabanpoor, M.A. Hossain, R.J. Clark, P.J. Ryan, D.J. Craik, A.L. Gundlach, J.D. Wade, R.A. Bathgate, K.J. Rosengren, Design, synthesis, and characterization of a single-chain peptide antagonist for the relaxin-3 receptor RXFP3, J. Am. Chem. Soc. 133 (13) (2011) 4965–4974.
[31] W.J. Zhang, X. Luo, G. Song, X.Y. Wang, X.X. Shao, Z.Y. Guo, Design, recombinant expression and convenient A-chain N-terminal europium-labelling of a fully active human relaxin-3 analogue, FEBS J. 279 (8) (2012) 1505–1512.
[32] C. Kuei, S. Sutton, P. Bonaventure, C. Pudiak, J. Shelton, J. Zhu, D. Nepomuceno, J. Wu, J. Chen, F. Kamme, M. Seierstad, M.D. Hack, R.A. Bathgate, M.A. Hossain, J.D. Wade, J. Atack, T.W. Lovenberg, C. Liu, R3(BDelta23 27)R/I5 chimeric peptide, a selective antagonist for GPCR135 and GPCR142 over relaxin receptor LGR7: in vitro and in vivo characterization, J. Biol. Chem. 282 (35) (2007) 25425–25435.
[33] J.L. LaBelle, S.G. Katz, G.H. Bird, E. Gavathiotis, M.L. Stewart, C. Lawrence, J.K. Fisher, M. Godes, K. Pitter, A.L. Kung, L.D. Walensky, A stapled BIM peptide overcomes apoptotic resistance in hematologic cancers, J. Clin. Invest. 122 (6) (2012) 2018–2031.
[34] G. Dawe, T. Jayakody, S. Marwari, Stapled B chain analogues of relaxin-3 retain biological activity, The FASEB Journal 30 (Suppl) (2016) lb512.
[35] R.A. Bathgate, M.H. Oh, W.J. Ling, Q. Kaas, M.A. Hossain, P.R. Gooley, K.J. Rosengren, Elucidation of relaxin-3 binding interactions in the extracellular loops of RXFP3, Front. Endocrinol. 4 (2013) 13.
[36] K.J. Rosengren, F. Lin, R.A. Bathgate, G.W. Tregear, N.L. Daly, J.D. Wade, D.J. Craik, Solution structure and novel insights into the determinants of the receptor specificity of human relaxin-3, J. Biol. Chem. 281 (9) (2006) 5845–5851.
[37] D. Shivakumar, E. Harder, W. Damm, R.A. Friesner, W. Sherman, Improving the prediction of absolute solvation free energies using the next generation OPLS force field, J. Chem. Theory Comput. 8 (8) (2012) 2553–2558.
[38] E. Harder, W. Damm, J. Maple, C. Wu, M. Reboul, J.Y. Xiang, L. Wang, D. Lupyan, M.K. Dahlgren, J.L. Knight, J.W. Kaus, D.S. Cerutti, G. Krilov, W.L. Jorgensen, R. Abel, R.A. Friesner, OPLS3: a force field providing broad coverage of drug-like small molecules and proteins, J. Chem. Theory Comput. 12 (1) (2016) 281–296.
[39] J.R. Kumita, D.G. Flint, O.S. Smart, G.A. Woolley, Photo-control of peptide helix content by an azobenzene cross-linker: steric interactions with underlying residues are not critical, Protein Eng. 15 (7) (2002) 561–569.
[40] J.R. Kumita, O.S. Smart, G.A. Woolley, Photo-control of helix content in a short peptide, Proc. Natl. Acad. Sci. U. S. A. 97 (8) (2000) 3803–3808.
[41] J.P. Lee, C. Liu, T. Li, G. Zhu, X. Li, Development of stapled helical peptides to perturb the Cdt1-Mcm6 interaction, J. Pept. Sci. 21 (7) (2015) 593–598.
[42] R. Lakshminarayanan, I. Yoon, B.G. Hegde, D. Fan, C. Du, J. Moradian-Oldak, Analysis of secondary structure and self-assembly of amelogenin by variable temperature circular dichroism and isothermal titration calorimetry, Proteins 76 (3) (2009) 560–569.
[43] N.J. Greenfield, Using circular dichroism collected as a function of temperature to determine the thermodynamics of protein unfolding and binding interactions, Nat. Protoc. 1 (6) (2006) 2527–2535.
[44] N.J. Greenfield, Circular dichroism analysis for protein–protein interactions, Methods Mol. Biol. 261 (2004) 55–78.
[45] N.J. Greenfield, Analysis of circular dichroism data, Methods Enzymol. 383 (2004) 282–317.
[46] C.N. Pace, T. McGrath, Substrate stabilization of lysozyme to thermal and guanidine hydrochloride denaturation, J. Biol. Chem. 255 (9) (1980) 3862–3865.
[47] H. Schagger, Tricine-SDS-PAGE, Nat. Protoc. 1 (1) (2006) 16–22.
[48] Y. Shaul, R. Seger, et al., The detection of MAPK signaling, in: Frederick M. Ausubel (Ed.), Current Protocols in Molecular Biology, 2006, p. 12, Chapter 18, Unit 18.
[49] G.L. Harris, M.B. Creason, G.B. Brulte, D.R. Herr, In vitro and in vivo antagonism of a G protein-coupled receptor (S1P3) with a novel blocking monoclonal antibody, PLoS One 7 (4) (2012) e35129.
[50] B.T. Mott, R.T. Eastman, R. Guha, K.S. Sherlach, A. Siriwardana, P. Shinn, C. McKnight, S. Michael, N. Lacerda-Queiroz, P.R. Patel, P. Khine, H. Sun, M. Kasbekar, N. Aghdam, S.D. Fontaine, D. Liu, T. Mierzwa, L.A. Mathews-Griner, M. Ferrer, A.R. Renslo, J. Inglese, J. Yuan, P.D. Roepe, X.Z. Su, C.J. Thomas, High-throughput matrix screening identifies synergistic and antagonistic antimalarial drug combinations, Sci. Rep. 5 (2015) 13891.
[51] C. Bagutti, B. Stolz, R. Albert, C. Bruns, J. Pless, A.N. Eberle, [111In]-DTPA-labeled analogues of alpha-melanocyte-stimulating hormone for melanoma targeting: receptor binding in vitro and in vivo, Int. J. Cancer 58 (5) (1994) 749–755.
[52] J. Inglese, P. Samama, S. Patel, J. Burbaum, I.L. Stroke, K.C. Appell, Chemokine receptor-ligand interactions measured using time-resolved fluorescence, Biochemistry 7 (8) (1998) 2372–2377.
[53] O. Mazor, M. Hillairet de Boisferon, A. Lombet, A. Gruaz-Guyon, B. Gayer, D. Skrzydelsky, F. Kohen, P. Forgez, A. Scherz, W. Rostene, Y. Salomon, Europium-labeled epidermal growth factor and neurotensin: novel probes for receptor-binding studies, Anal. Biochem. 301 (1) (2002) 75–81.
[54] L.M. Haugaard-Kedstrom, L.L. Wong, R.A. Bathgate, K.J. Rosengren, Synthesis and pharmacological characterization of a europium-labelled single-chain antagonist for binding studies of the relaxin-3 receptor RXFP3, Amino Acids 47 (6) (2015) 1267–1271.
[55] R. Taussig, J.A. Iniguez-Lluhi, A.G. Gilman, Inhibition of adenylyl cyclase by Gi alpha, Science (New York, N.Y.) 261 (5118) (1993) 218–221.
[56] I. Litosch, T.H. Hudson, I. Mills, S.Y. Li, J.N. Fain, Forskolin as an activator of cyclic AMP accumulation and lipolysis in rat adipocytes, Mol. Pharmacol. 22 (1) (1982) 109–115.
[57] S. Wada, T. Urase, Y. Hasegawa, K. Ban, A. Sudani, Y. Kawai, J. Hayashi, H. Urata, Aib-containing peptide analogs: cellular uptake and utilization in oligonucleotide delivery, Bioorg. Med. Chem. 22 (24) (2014) 6776–6780.
[58] Y. Demizu, M. Tanaka, M. Doi, M. Kurihara, H. Okuda, H. Suemune, Conformations of peptides containing a chiral cyclic alpha, alpha-disubstituted alpha-amino acid within the sequence of Aib residues, J. Pept. Sci. 16 (11) (2010) 621–626.
[59] S. Wada, Y. Hashimoto, Y. Kawai, K. Miyata, H. Tsuda, O. Nakagawa, H. Urata, Effect of Ala replacement with Aib in amphipathic cell-penetrating peptide on oligonucleotide delivery into cells, Bioorg. Med. Chem. 21 (24) (2013) 7669–7673.
[60] S. Wada, H. Tsuda, T. Okada, H. Urata, Cellular uptake of Aib-containing amphipathic helix peptide, Bioorg. Med. Chem. Lett. 21 (19) (2011) 5688–5691.
[61] L.D. Walensky, A.L. Kung, I. Escher, T.J. Malia, S. Barbuto, R.D. Wright, G. Wagner, G.L. Verdine, S.J. Korsmeyer, Activation of apoptosis in vivo by a hydrocarbon-stapled BH3 helix, Science (New York, N.Y.) 305 (5689) (2004) 1466–1470.